Converted Photons in the Search for Photon-Jets from Light Axion-Like Particles

REU Program at Columbia University - Nevis Labs

Lyra Bornholdt-Collins[1]

[1]Tufts University

August 6, 2026

Nevis Laboratories
Columbia University

Abstract

This is a report of a study on converted photons as background in the search for light axion-like particles (ALPs), using data from Run 3 collected in 2022 from the ATLAS detector at the Large Hadron Collider. This study analyzed and assessed the performance of a custom transformer, the purpose of which was to identify ALP decay signature and distinguish it from background processes (such as converted photons). This study showed that converted photons were not always treated as background to the ALP decay signal process by the transformer. These findings necessitate revisiting the training of the transformer.

Contents

1 Introduction

1.1 The Standard Model

The Standard Model (SM) of particle physics is the theoretical framework which best describes the most fundamental building blocks of the universe. The SM separates fundamental particles into classes of fermions and bosons. Fermions are considered as the fundamental units of matter and are further classed as quarks and leptons. Bosons are force carriers and are responsible for the four fundamental forces (the weak force, the strong force and the electromagnetic force[1]) [8].

Although the SM accounts for much of what has been observed of particle physics through experimentation, there are still many questions it leaves unanswered. For example, it is well established through observations in astrophysics that most of the matter in the universe does not consist of the particles outlined in the SM. This matter does not interact through the same modes as the documented particles in the SM, and hence is dubbed "Dark Matter". Theorized particles that live outside the SM are characterized as Beyond the Standard Model (BSM), and are the subject of many ongoing experimental searches.

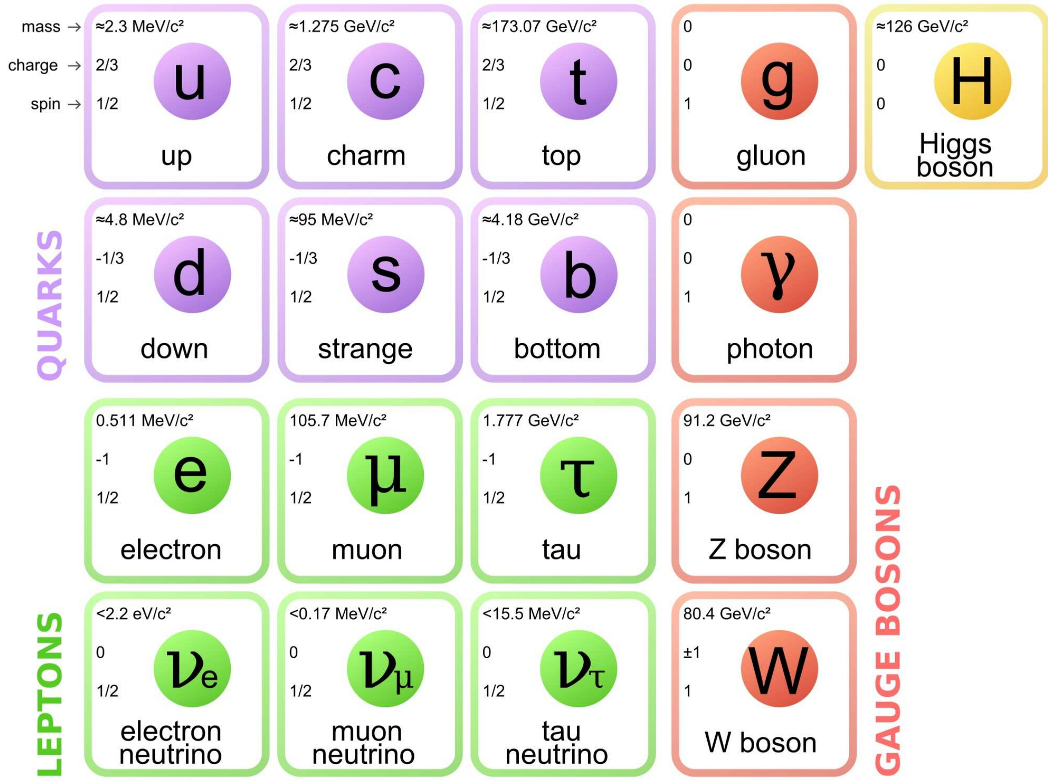

Figure 1: *The Standard Model of particle physics.*

1.2 Instrumentation

1.2.1 The Large Hadron Collider

The Large Hadron Collider (LHC) operates through CERN in Geneva, Switzerland, and is the largest particle accelerator in the world. Along its 27 km ring, the LHC accelerates protons at 99.999999% of the speed of light in two separate beam pipes traveling in opposite directions. The protons in the beams are able to move in this circular ring due to very strong superconducting magnets (cryodipoles) that guide the beams. At four set locations along the ring, the protons

[1]The fourth fundamental force, gravity, does not fit within the SM – one of its many mysteries still to uncover.

collide. At these major collision points are the particle detectors: ATLAS, CMS, ALICE and LHCb.

1.2.2 The ATLAS Detector

Of these four particle detectors at the LHC, ATLAS is the largest in both size and number of collaborators. With more than 5,000 collaborators from over 180 different institutions, the ATLAS experiment is one of the largest collaborative experiments in any field of science to date. The detector itself spans 46 meters long and 25 meters in diameter. It records high energy particle collisions at a rate of 40 mHz, which equates to more than one billion interactions every second. The ATLAS detector is one of two general detectors at the LHC (the other being CMS), meaning it is used for many different studies. Notably, the ATLAS detector was instrumental in the discovery of the Higgs boson in 2012, the theorization for which the Nobel prize was awarded in 2013.

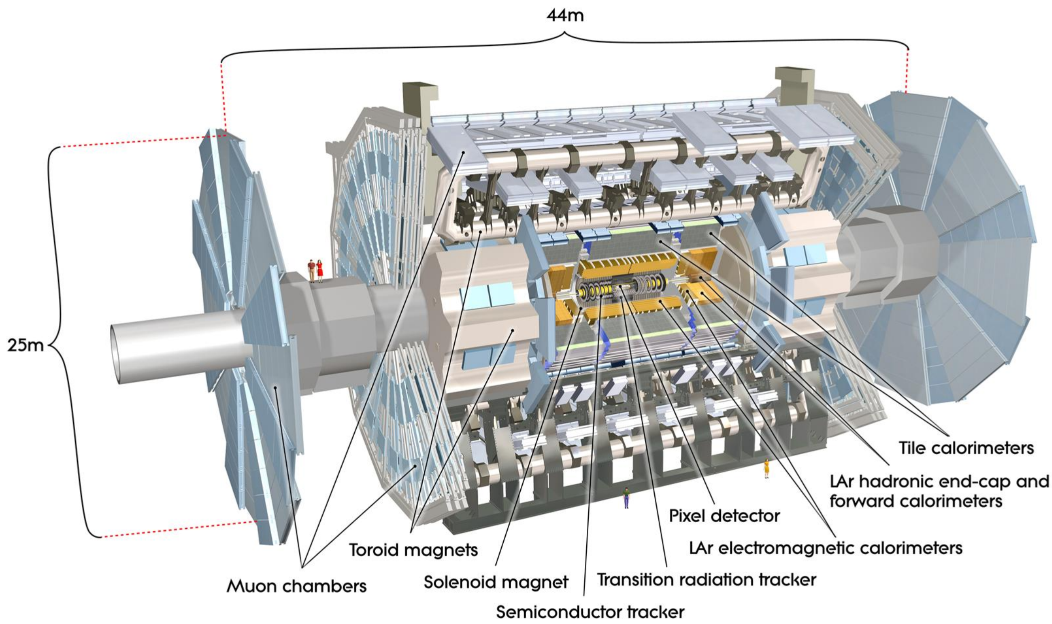

Figure 2: *The ATLAS detector.*

The ATLAS detector employs the use of several unique variables in order to better describe its layout. This paper focused on the transverse momentum (p_T), pseudorapidity (η) and the azimuthal angle (ϕ). The transverse momentum describes the component of a particle which is perpendicular to the beamline. Pseudorapidity is a calculated variable from the angle theta between the x and y axes that follows the equation $\eta = -ln[tan(\theta/2)]$. It describes the angle of the particle's trajectory relative to the beamline (the tilt from the beam axis), where 0 represents a trajectory perpendicular to the beam. The azimuthal angle is angle measured around the beam axis in the x-y plane, and can be seen in Fig. 3.

The ATLAS detector is made up of the Inner Detector, the calorimeter, and the Muon Spectrometer. The Inner Detector, as seen in Fig. 4, has a radius of a little over one meter and is the first part of ATLAS that sees decay products from the collisions inside the detector. Its main components are the Pixel Detector, the Semiconducting Tracker (SCT), and the Transition Radiation Tracker (TRT). These layers serve the purpose of measuring the direction, momentum and charge of the particles produced in each collision [7].

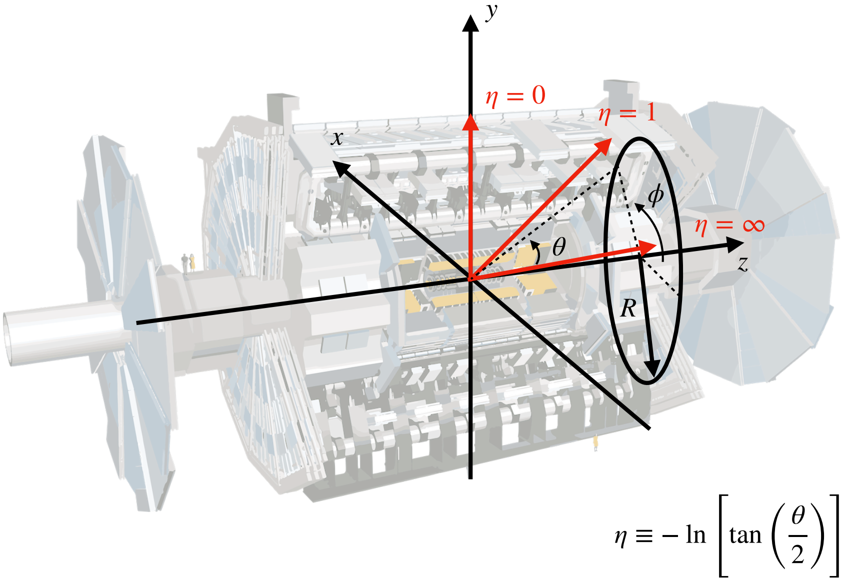

Figure 3: *The detector overlaid with the coordinate system employed by ATLAS.*

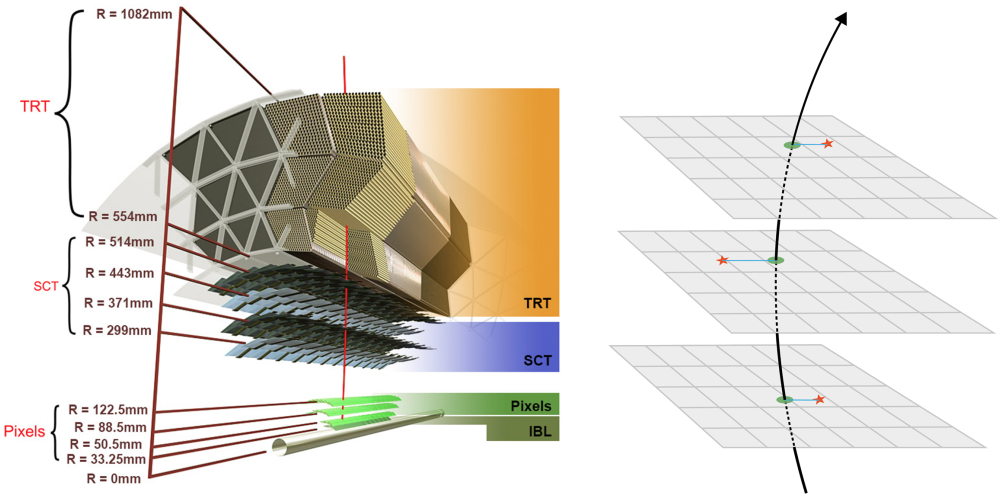

Figure 4: *Cross section of the Inner Detector (ID).*

The ATLAS Electromagnetic Calorimeter system measures the energy that particles lose as they pass through the detector. The Liquid Argon (LAr) electromagnetic calorimeter (see Fig. 5) surrounds the inner detector and uses layers of metal to absorb incoming particles, which then ionize with the liquid argon between layers to produce an electric current. To keep the argon in liquid form, it must be kept at an extremely low temperature. The electric current can be translated into an associated energy of the object, and given the information about which cells read out that energy, also reflects the spatial positioning of the particle within the detector. The other main calorimeter system is the Hadronic calorimeter, which surrounds the LAr calorimeter and detects any energy from particles that has not already been deposited in the LAr calorimeter [5].

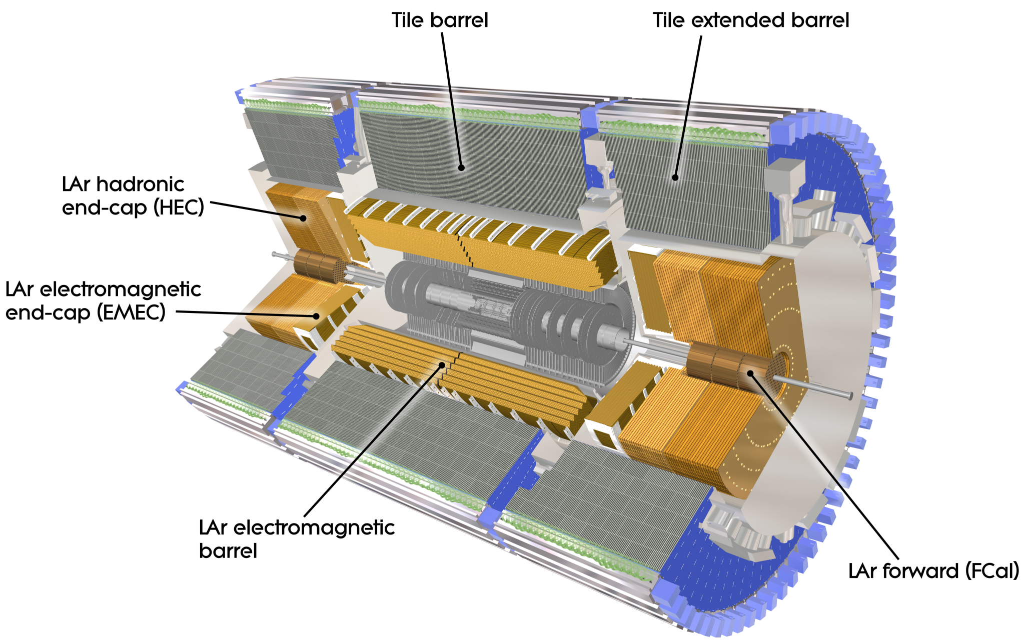

Figure 5: *The Liquid Argon (LAr) Electromagnetic Calorimeter.*

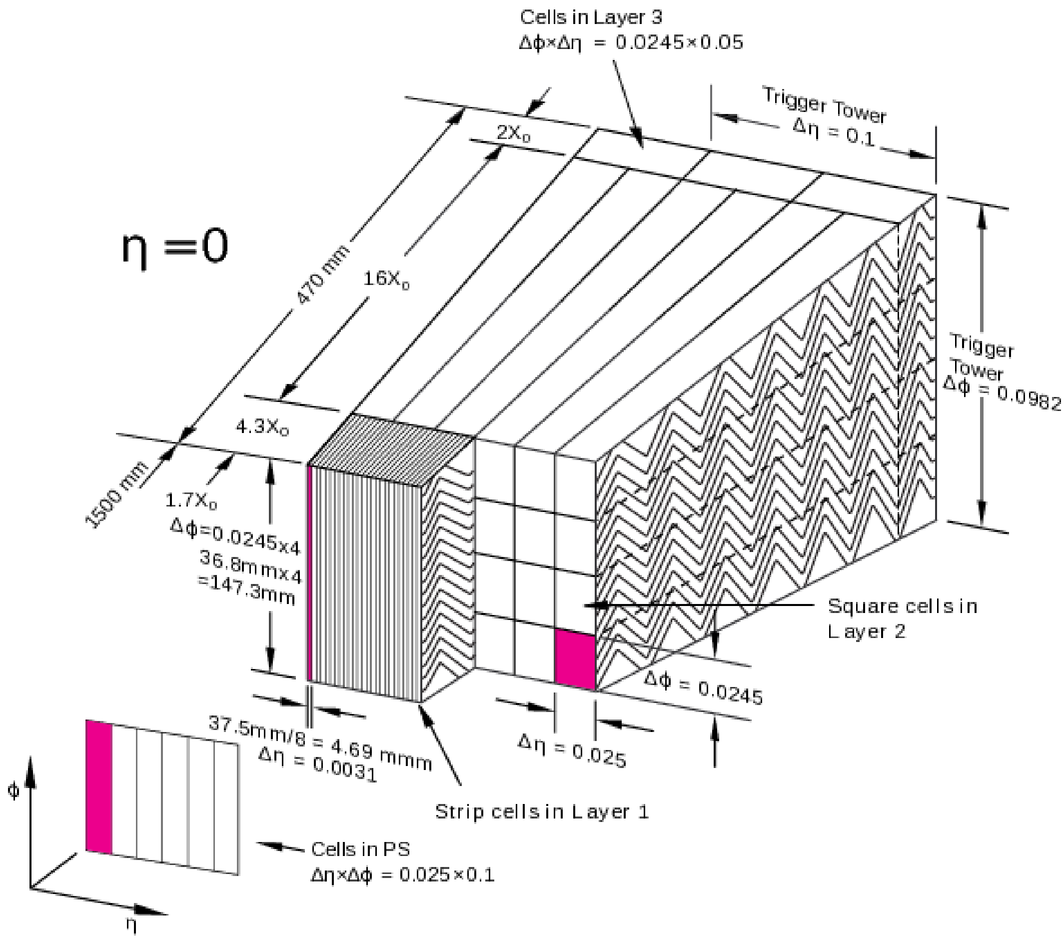

Figure 6: *Layers of the LAr Electromagnetic Calorimeter [13].*

The LAr electromagnetic calorimeter is comprised of a presampling layer and three subsequent layers. Together, these layers have just under 200,000 energy-reading cells, as seen in Fig. 6. The presampler (PS) serves to measure the energy of the objects before it is lost to the calorimeter. The front layer is the most finely segmented in η which increases the precision of spatial measurements made in the calorimeter and helps to distinguish $\pi^0 \to \gamma\gamma$ from γ. The middle layer is the longest and has a characteristic accordion structure which guarantees that no particle escapes undetected. The purpose of the final back layer is to catch the tail end of showers.

The final component of the ATLAS detector is the muon spectrometer. The muon spectrometer is the most outer layer of the detector, and its purpose is to measure muons [6]. Muons are much heavier particles than photons, and so this part of the detector was not central to this study.

2 Search for Photon-jets from $X \to 2a \to 4\gamma$

2.1 Axions

One question that arises from the SM is Charge-Parity (CP) violation and the strong CP problem. CP violation is the breaking of charge conjugation parity symmetry, which states that the laws of physics should be the same for a particle if it is switched with its associated antiparticle counterpart, with spatial coordinates inverted (as in a mirror). This symmetry has been shown to be broken by weak interactions and theoretically should also hold true for strong interactions. This has not yet been experimentally observed, hence it is dubbed "the strong CP problem".

One solution to the strong CP problem proposed in 1978 was the existence of a new type of particle called an axion. The name "axion" was chosen because it was shared with a brand of laundry detergent, and the existence of this particle would perfectly "clean up" the strong CP problem. Although searches for the QCD axion are ongoing, no experimental evidence has yet been found to support its existence. However, there are still ongoing searches for similar theorized particles, which are classified as axion-like particles.

2.2 Axion-like Particles

Axion-like particles (ALPs) are dark matter candidates with a strong theoretical backing. The object of this search is the identification of light ALPs with with a di-photon decay signature. Fig. 7 shows a Feynman diagram of the light ALP decay process. The parent particle, X, has an unknown scalar mass that is significantly more massive than the daughter ALPs. One possible parent particle for this process is the Higgs boson, but it could also be another known particle, or even a new particle existing in the dark sector. As these are light ALPs, they have a very small mass (on the order of 100 MeV). The large difference in the mass of the parent particle and the mass of the ALPs means that they have high energy. There is also a large difference in the massless photon pair and the ALP mass, so these photons also have very high energy and are considered "boosted" photons. This makes these photons highly collimated, meaning that the two photons have a very small angle of separation.

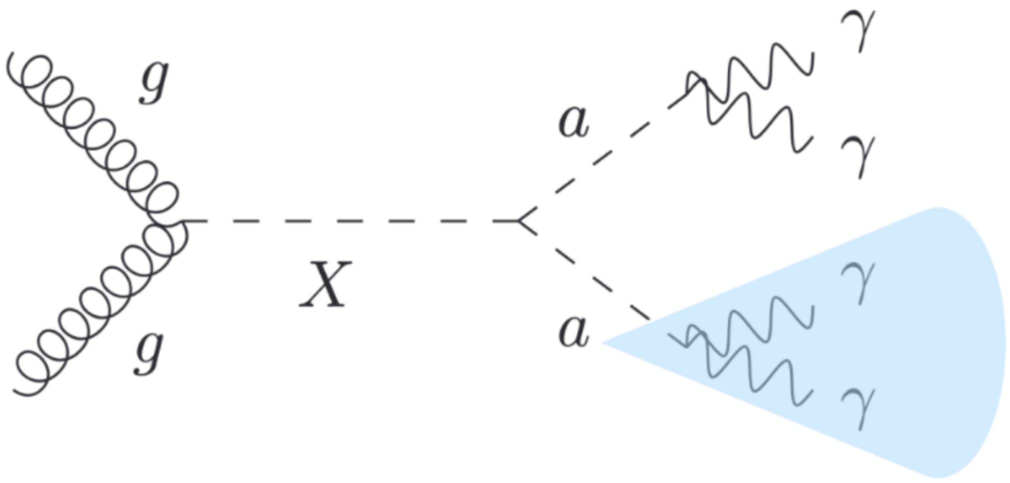

Figure 7: *Feynman diagram of the light ALP decay process. It depicts two gluons forming the parent particle, labeled "X". This decays into the two daughter ALPs "a" which each decay into a pair of collimated photons.*

2.3 The Transformer

As the diphoton ALP decay signature is highly collimated, it resembles a host of other backgrounds. This includes but is not limited to single photons in the calorimeter, as pictured in Fig. 8. Here, you can see a cartoon rendition of what a single photon versus the collimated photon-jet looks like in ATLAS' electromagnetic calorimeter. In order to combat the difficulty in distinguishing these processes, a transformer was developed in part by the ATLAS group at Columbia University [10].

A transformer is a machine learning model that can track relationships in sequential data. The architecture of this transformer is outlined in Fig. 9. The input to the transformer is real data directly from the cells of the calorimeter. The transformer then processes that data and runs it through a classifier network. Here, each event is assigned a score on a scale of 0 to 1, with 0 corresponding to an event classified as background and 1 corresponding to an event considered as ALP signal.

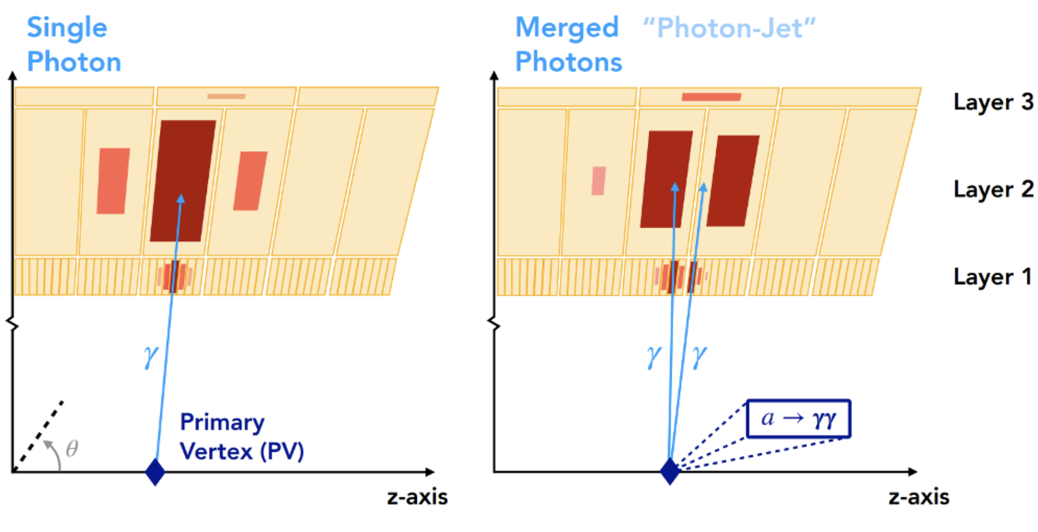

Figure 8: *Single photons vs. merged photons (photon-jets) in the electromagnetic calorimeter.*

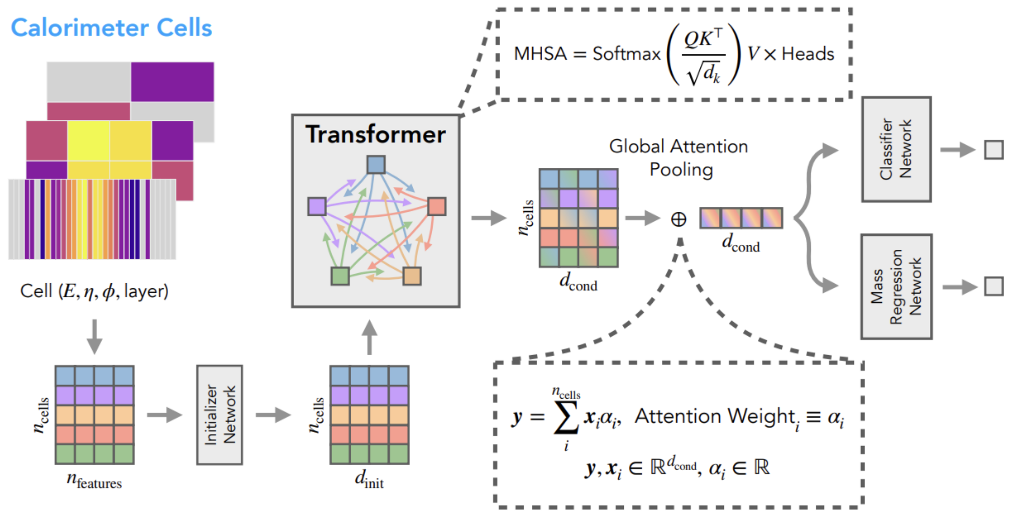

Figure 9: *Architecture of the transformer model.*

Fig. 10 shows the preliminary performance of the transformer during its training phase. The colorful blue and yellow lines represent different possible ALP masses ranging from 0.1 GeV to 10 GeV. These plots show transformer scores from Monte Carlo simulated data using Geant4 and explore what data would look like if there was an ALP of a particular mass present. Each of these peak higher at 1.0, signifying that the transformer is behaving correctly in this preliminary training, as it is identifying each of these different possible ALP masses as signal. The black line shows how the transformer behaves on single photons. It distinctly peaks at 0, indicating that the transformer was able to distinguish this single photon signature as background to the ALP signal.

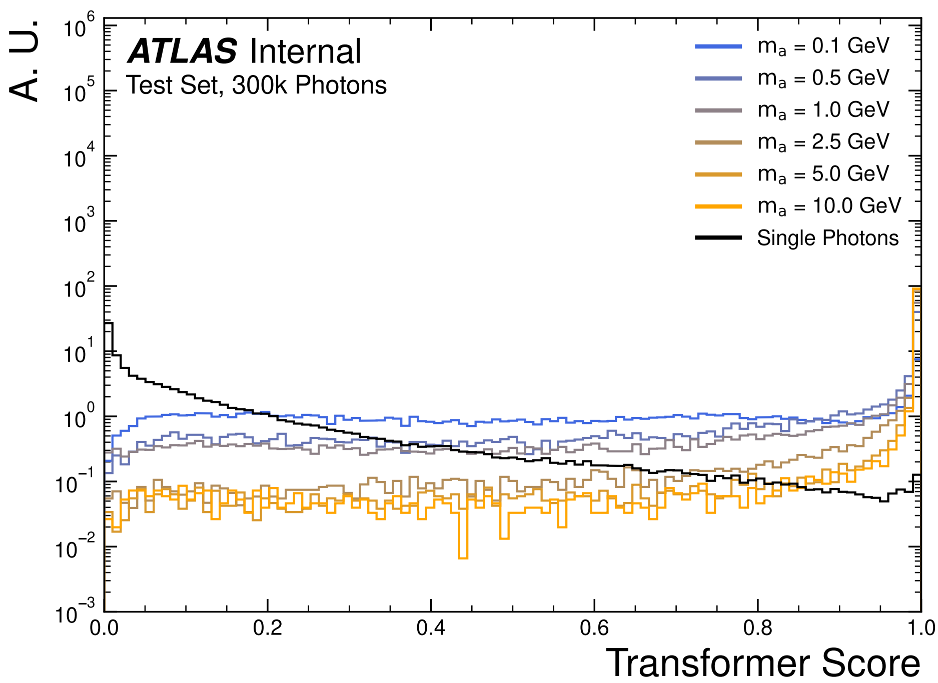

Figure 10: *Preliminary transformer scores taken from the training of the transformer. Blue through yellow lines indicate different masses of ALPs being probed. The black line represents single photons which are considered background to the ALP signal.*

2.4 Converted Photons

In order to validate the transformer, this study focuses on another background - the converted photon - to further assess the transformer behavior. As photons are massless particles, in order to conserve energy and momentum they are completely stable and do not spontaneously decay or evolve. However, photons can interact with other material and thereby convert. Converted photons occur around twenty-five percent of the time when a photon comes into contact with some material in the ATLAS detector. Fig. 11 shows a converted photon from the left coming into contact with some nucleus (here representing the detector material) and then converting into an electron-positron pair. This electron pair is highly collimated, which is why this process looks very similar to the ALP diphoton decay signature.

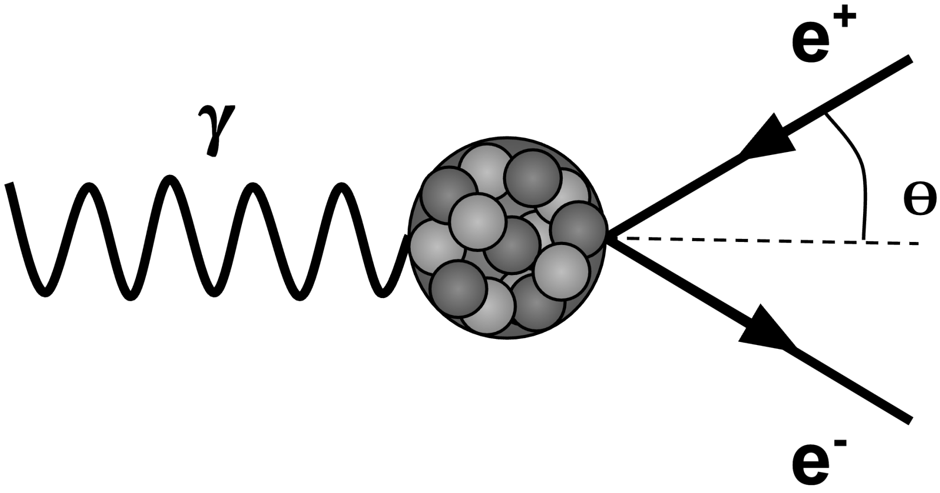

Figure 11: *Feynman diagram of a converted photon.*

Fig. 12 shows an ATLAS event display of what this converted photon looks like in the detector. The brown dot denotes the vertex of the photon conversion, which correlates to the second layer of the Pixel Tracker in the Inner Detector. The blue line coming out of the vertex of conversion shows the path of the electron, and the red line shows the path of the positron. The yellow band at the right-hand edge of the event display shows the beginning of the converted photon in the electromagnetic calorimeter. As mentioned, this conversion vertex corresponds exactly with the location of the Pixel Tracker; as the tracker is made up of material, it allows the photon to convert when it comes into contact with the tracker.

Two converted photons are shown in another event display in Fig. 13, which is zoomed out so that the focus is on the calorimeter. The two converted photons are shown in transparent green bands at the top-right and left of the image. The solid green rectangles beneath the bands show the cell-level energy deposits from the converted photons in the calorimeter.

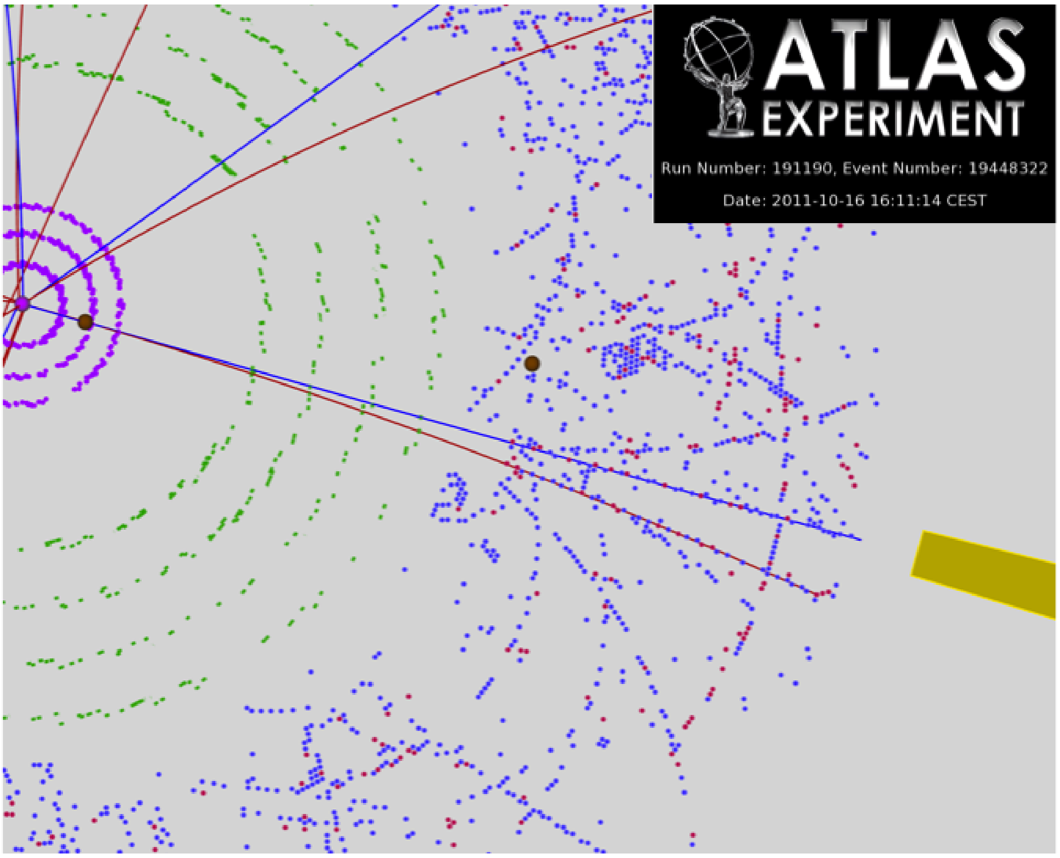

Figure 12: *An ATLAS event display showing the vertex of conversion of a converted photon located in the second layer of the pixel tracker.*

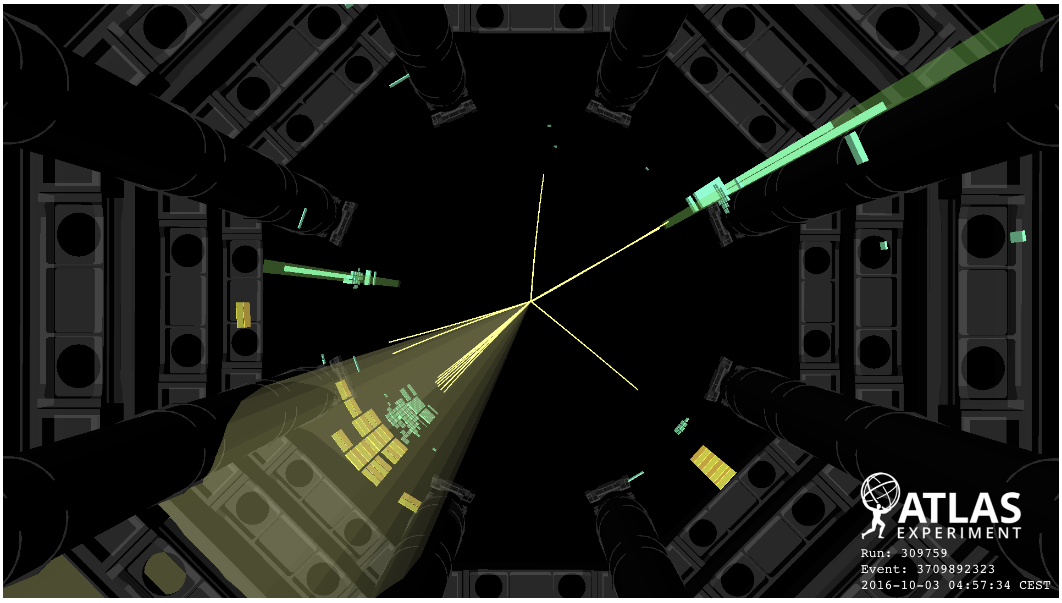

Figure 13: *An ATLAS event display showing two converted photons (seen here as transparent green bands) in the electromagnetic calorimeter.*

3 Converted Photons as Background

3.1 Material Mapping of the Inner Detector

In order to examine converted photons' behavior in the transformer, it was first necessary to verify the correct identification of converted photons in the detector. As photons only convert in the presence of some material in the detector, by mapping the vertices of conversion for converted photons it should be possible to reconstruct what resembles a map of the inner detector. Any points not corresponding to an area in which there is known material in the detector would indicate that these photons are not converted. Fig. 14 is a plot of the vertices of conversion in the x-y plane of the detector. This plot shows three clear rings in red that correspond directly to the radii from the beam of the first three layers of the pixel tracker in the Inner Detector. The octagon makes up the support structure for the SCT is also clearly visible. At the very edge of this plot (which has a cutoff of 300 mm) is also the edge of the inner layer of the SCT. As there are no vertices outside of the area that is known to house detector material, this affirms the correct identification of converted photons.

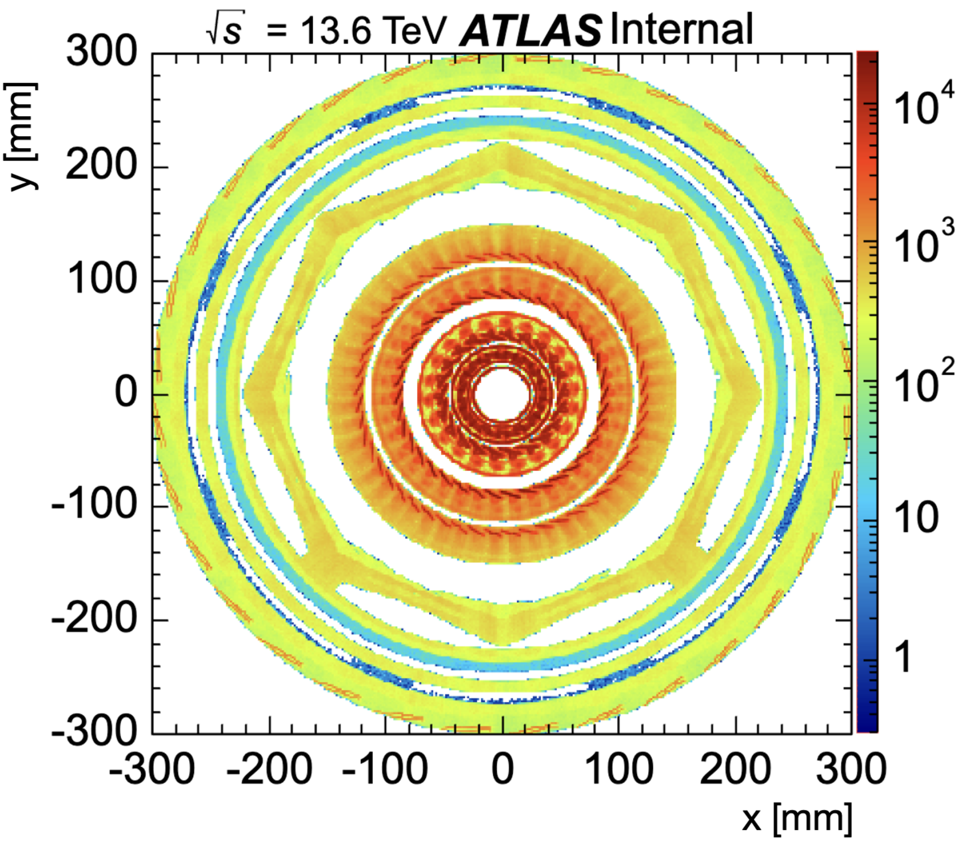

Figure 14: *Map of the vertices of conversion for converted photons in the x-y plane.*

3.2 Transformer Scores

3.2.1 Monte Carlo Simulated ALP Signal

After the ability to identify converted photons in the detector was confirmed, the performance of the transformer score for the Monte Carlo simulated signal sample was analyzed. Fig. 15 shows potential parent particles of masses ranging from 200 GeV to 2500 GeV and potential ALP masses ranging from 2.5 GeV to 10.0 GeV. In each of these plots there are cuts placed on p_T so that it is greater than 20 GeV and cuts in η so that $|\eta| < 2.37$ in addition to an exclusion of the crack in the detector. There is also a cut included so that there are two photons in each event, ensuring that these are signal-like events because the ALP decay is of two collimated photons. These plots are normalized by area ($area = 1$) so that they are comparable by shape. Each of these plots peaks significantly at 1.0 in the transformer score, indicating that the transformer correctly identifies the presence of the ALP for each of these different masses. In blue are the unconverted photons in the signal sample, and in red are the converted photons in the signal sample. Of these two, the unconverted photons behave more background-like relative to the converted photons, which further motivates looking at single converted photons as background to the ALP signal in this study.

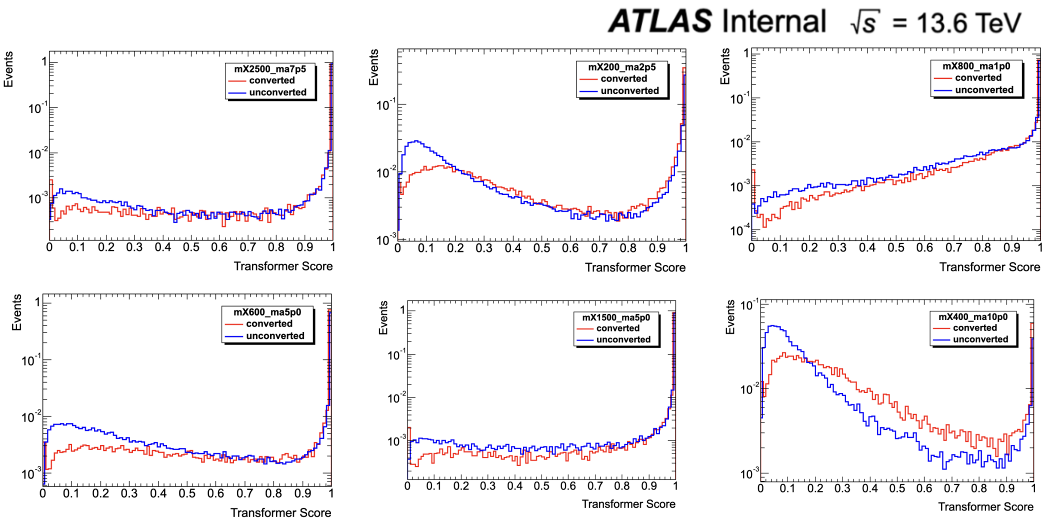

Figure 15: *Transformer scores for Monte Carlo signal sample. From left to right and top to bottom: mX = 2500 ma = 7.5 GeV, mX = 200 GeV ma = 2.5 GeV, mX = 800 GeV ma = 1.0 GeV, mX = 600 GeV ma = 5.0 GeV, mX = 1500 GeV ma = 5.0 GeV, mX = 400 GeV ma = 10.0 GeV.*

3.2.2 Converted and Unconverted Photons from Data

Fig. 16 shows the transformer scores of converted and unconverted photons from data collected in 2022 from Run 3 of the LHC. In addition to the same cuts on p_T and η as the MC signal sample plots, there were additional cuts so that each of these events was isolated, and a check so that these events were all matched with the 140 GeV loose single photon trigger. For these plots, instead of a photon multiplicity cut of two photons to ensure the events are signal-like, there is also a cut so that there are only single photons present. This ensures that these events cannot be ALP signal, as those events will have two photons, and so verifies that these objects are single photons. Both the converted and unconverted photons peak significantly at 0.0 in the transformer score, indicating that these are being identified as background-like events in the transformer, as was intended. However, the converted photons look more background-like relative to the unconverted photons, which was not expected and differs from the transformer scores of the MC simulated plots.

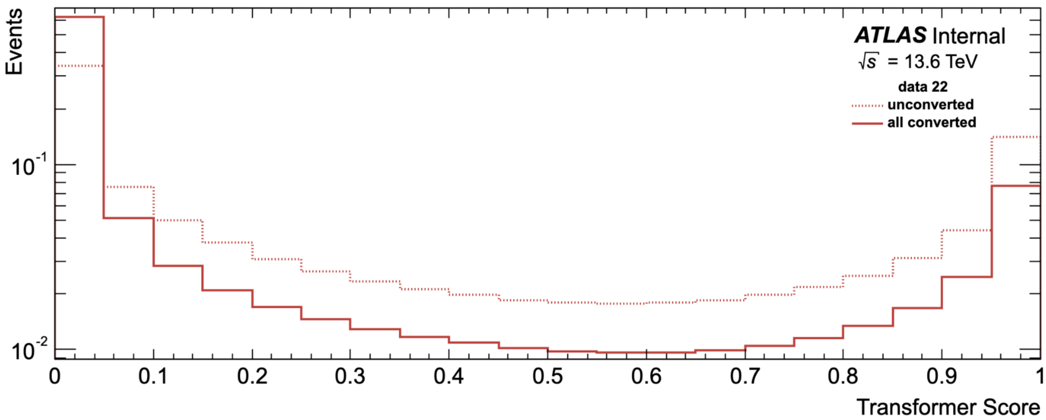

Figure 16: *Transformer scores from data showing the behavior of converted and unconverted photons. Converted photons are shown in solid red and unconverted photons are shown in dashed red line.*

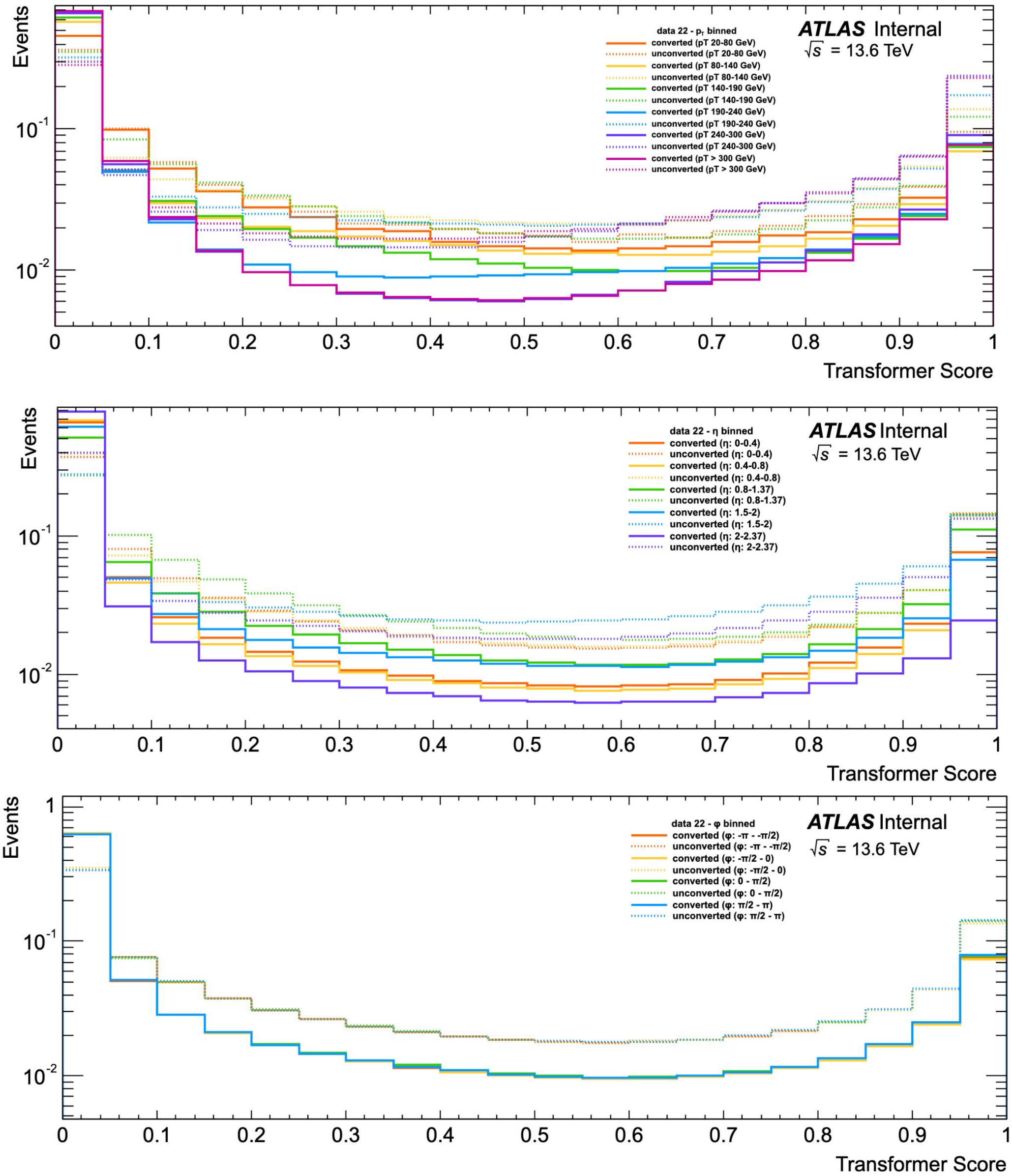

Figure 17: *Transformer scores from data binned by the kinematic variables p_T (top), η (middle) and ϕ (bottom).*

3.2.3 Kinematic Variables

Identifying the cause of this discrepancy in transformer score between the unconverted and converted photons required analyzing the dependence of each on the kinematic variables used in the ATLAS detector. Fig. 17 shows the transformer scores for each of the kinematic variables p_T, η and ϕ. In ϕ there is no visible variation across the four bins, and so it is safe to conclude there is no dependence here. This was expected as ϕ should be symmetric across all values in the detector. However, there is clear variation across bins in p_T and those in η. As these plots are trigger matched to the 140 GeV trigger, the p_T bins below 140 GeV can be disregarded. With this in mind, there is a slight out-performance of higher p_T converted photons as background, but unconverted photons appear even more signal-like at higher p_T. In η, there is no clear correlation between more forward bins and more central bins.

3.2.4 Photon Identifications

In addition to examining kinematic variables, it was also important to consider the photon identification criteria. ATLAS has a set of parameters outlined in Fig. 18 for what is considered a photon [2]. There are three levels of parameters that a photon must meet to be classified as such by ATLAS: loose, medium and tight. These vary in their stringency and are nested labels so that tight and medium labels are included within loose and the tight label is included within the medium label.

Category	Description	Name	Loose	Tight
Acceptance	$\|\eta\| < 2.37$, $1.37 < \|\eta\| < 1.52$ excluded	–	✓	✓
Hadronic leakage	Ratio of E_T in the first sampling of the hadronic calorimeter to E_T of the EM cluster (used over the range $\|\eta\| < 0.8$ and $\|\eta\| > 1.37$)	R_{had_1}	✓	✓
	Ratio of E_T in all the hadronic calorimeter to E_T of the EM cluster (used over the range $0.8 < \|\eta\| < 1.37$)	R_{had}	✓	✓
EM Middle layer	Ratio in η of cell energies in 3×7 versus 7×7 cells	R_η	✓	✓
	Lateral width of the shower	w_{η_2}	✓	✓
	Ratio in ϕ of cell energies in 3×3 and 3×7 cells	R_ϕ		✓
EM Strip layer	Shower width for three strips around strip with maximum energy deposit	$w_{s\,3}$		✓
	Total lateral shower width	$w_{s\,\mathrm{tot}}$		✓
	Energy outside core of three central strips but within seven strips divided by energy within the three central strips	F_{side}		✓
	Difference between the energy associated with the second maximum in the strip layer, and the energy reconstructed in the strip with the minimal value found between the first and second maxima	ΔE		✓
	Ratio of the energy difference associated with the largest and second largest energy deposits over the sum of these energies	E_{ratio}		✓

Figure 18: *Parameters outlined by ATLAS on loose and tight photon IDs [2].*

Fig. 19 shows the performance of the transformer in bins of these photon IDs. This plot shows that instead of a better (more background-like) score as the confidence in photon identification increases (from loose to tight), the transformer starts to treat the photons more like signal. Notably, the transformer also treats unconverted tight photons overall more like the ALP signal than as background. The tight photon identification being the most strict and certain of the event's status as a photon, this is a puzzling performance from the transformer. These most pure single photons are the objects that are most definitely not ALP signal, and yet these are the events that transformer treats as signal-like.

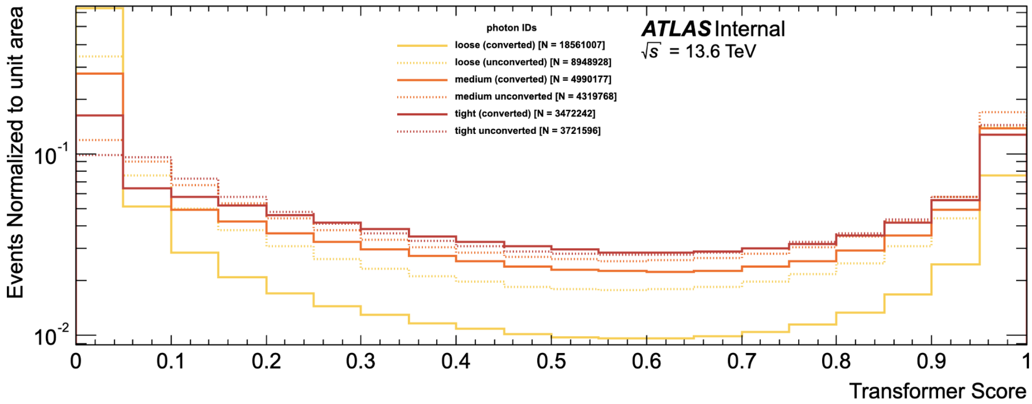

Figure 19: *Transformer scores for each photon identification type. In yellow are loose photons, orange are medium and red are tight, each with dashed lines representing the unconverted and solid lines indicating converted photons.*

3.2.5 $\gamma+$ Jets

In addition to transformer performance on converted photons from data and simulated ALP signal sample, this study also examined the behavior of the transformer on Monte Carlo simulated data of $\gamma+$ jets. Fig. 20 shows transformer scores for direct and fragmented $\gamma+$ jets for both converted and unconverted photons. Again, the plot shows that, while converted photons look clearly background-like, unconverted photons do not look significantly more background-like. Although unconverted photons peak slightly higher at 0.0 than 1.0, the difference is not substantial.

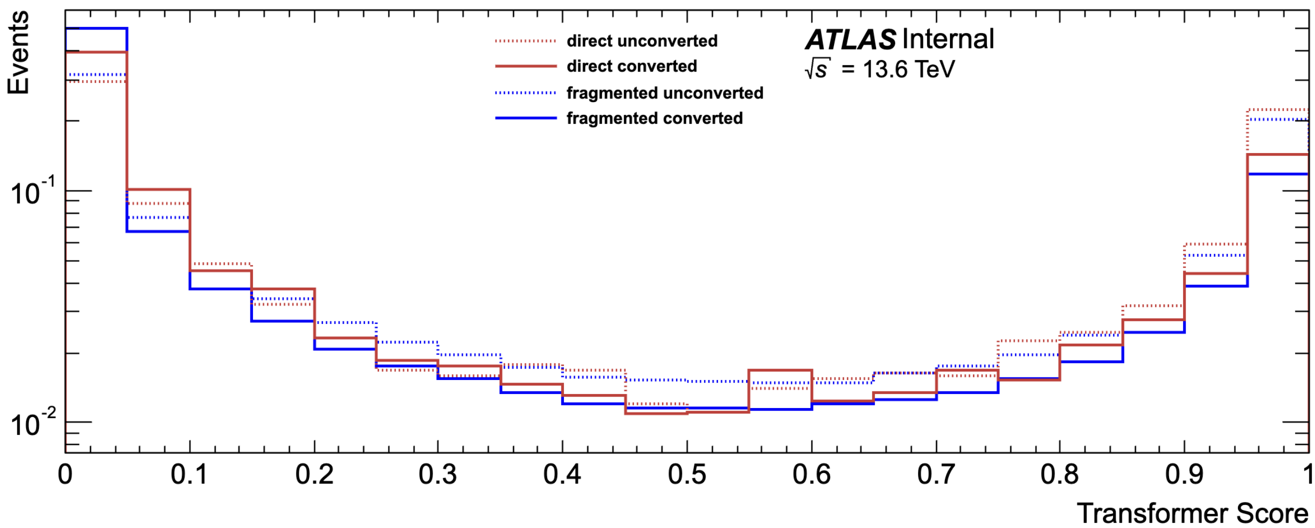

Figure 20: *Transformer scores for $\gamma+$ jets separated by fragmented (in blue) and direct (red) events.*

4 Conclusions

4.1 Background Efficiency

Eventually, when the transformer is implemented, a cut will be established to distinguish signal-like versus background-like objects. Fig. 21 shows the percentage of events preserved when making a cut at any particular transformer score. For example, a cut at a transformer score of 0.6 would correspond to preserving just under thirty percent of events. This can be compared to Fig. 22, which shows the signal efficiencies for the Monte Carlo simulated ALP signal for various parent-daughter mass pairings. Across the board these plots show a much higher percentage of data being kept at that same potential 0.6 transformer score cutoff.

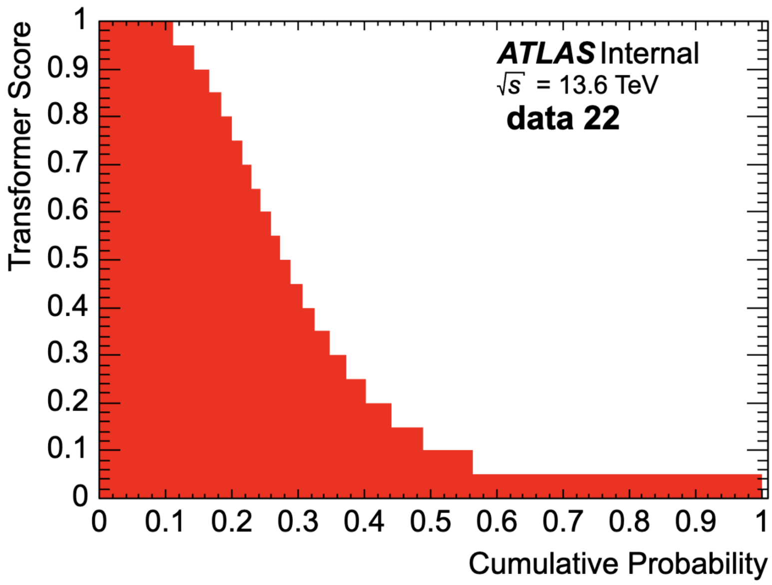

Figure 21: *Background efficiency of the transformer on data from Run 3 collected in 2022.*

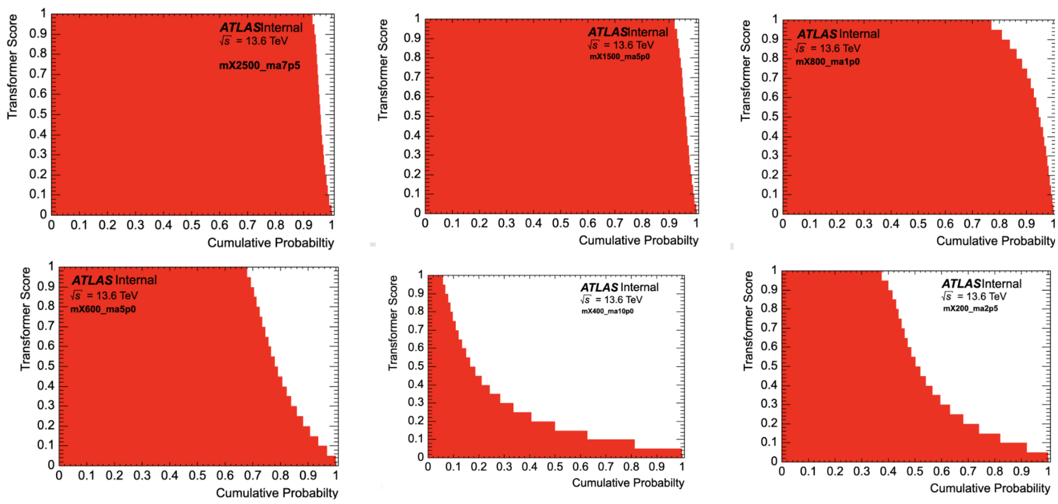

Figure 22: *Signal efficiency plots of cumulative probability for Monte Carlo simulated data for various parent-daughter mass pairings. From left to right, top to bottom: mX 2500 GeV ma 7.5 GeV, mX 1500 GeV ma 5.0 GeV, mX 800 GeV ma 1.0 GeV, mX 600 GeV ma 5.0 GeV, mX 400 GeV ma 10.0 GeV, mX 200 GeV ma 2.5 GeV.*

4.2 ROC curves

In addition to estimates of the efficiencies of the transformer, ROC curves were also generated to evaluate the transformer performance. Fig. 23 shows a ROC curve of the cumulative probability of preserving events in the background from data on the x-axis versus the cumulative probability from the signal sample of the 400 GeV parent mass with the 10.0 GeV ALP mass. If the cumulative probabilities were the same for the signal and background, it would result in a flat diagonal line following $y = x$, but as is, it is evident that there is a huge discrepancy between the signal and background transformer efficiencies.

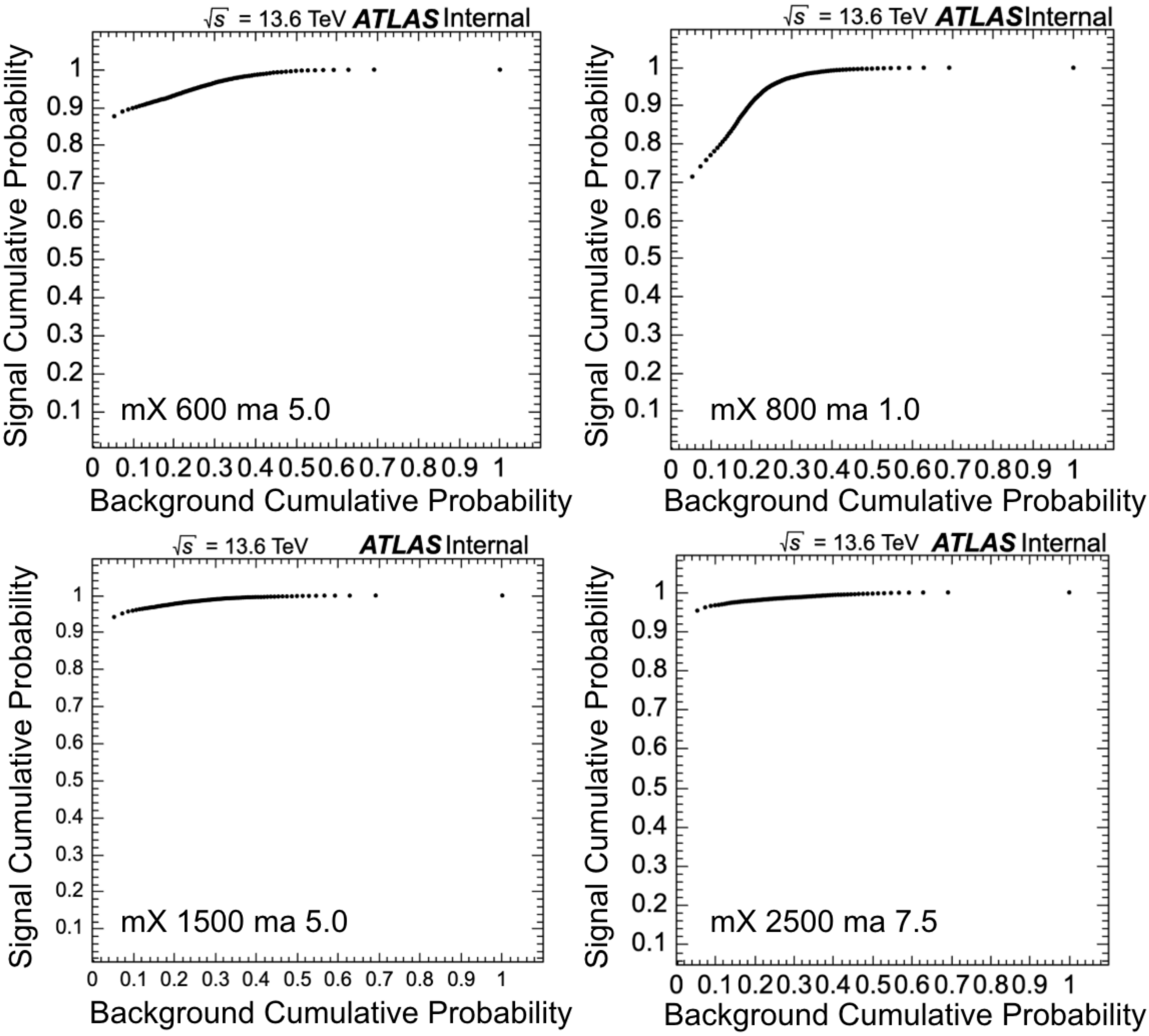

Figure 23: *ROC curves of background cumulative probability and signal cumulative probability for a range possible of parent and ALP mass pairings. From left to right, top to bottom: mX 600 GeV ma 5.0 GeV, mX 800 GeV ma 1.0 GeV, mX 1500 ma 5.0 GeV, mX 2500 ma 7.5 GeV.*

4.3 Future Work

Although there were no concrete answers as to why the transformer did not treat converted photons as expected, there was still much value to this study. More questions have been raised about the performance of the transformer on high p_T photons, as well as questions about the seemingly random variance in η. There is also more to explore with respect to photon identifications. One possible path to examine here is the photon isolation, to see if this is being correctly applied and if that has an impact on the transformer. Across all the different attributes of the photons that were explored in this study, it was clear that unconverted photons behaved more signal-like than the converted photons in the transformer, and in a few cases also behaved overall more signal-like than background-like. This in itself requires further consideration, as the converted photons had strong motivation to behave more like signal in the transformer, so it is possible there is some other process here that is causing the transformer to treat unconverted photons in this way.

One possible process that would be a logical next step in this project would be to examine the $Z \rightarrow \ell\ell\gamma$, also known as radiative Z decay [11]. This process also has two well-defined tracks, like the converted photon. This process provides a very pure photon sample, and so could provide answers especially to questions around the behavior of the transformer with the tight photon identification.

Ultimately, these findings necessitate revisiting the training of the transformer before moving forward with its implementation.

5 Acknowledgements

Thank you to everyone who made this experience possible. Thank you especially to Professor John Parsons, Professor Georgia Karagiorgi, Professor Reshmi Mukherjee, Amy Garwood and Asia Latt. Thank you also to Dr. Lauren Osojnak, Dr. Jonathan Long and Gabriel Matos for their help and guidance throughout this project. Thank you also to everyone from the Columbia ATLAS group, as well as our close collaborators at University of Texas at Austin and McGill University, for all their support. Lastly, thank you to my cohort of REU participants for cultivating an environment of curiosity and support that set the tone for an unforgettable summer research experience.

This material is based upon work supported by the National Science Foundation under Grant No. PHY-2349438.

References

[1] ATLAS Collaboration, *Electron and photon performance measurements with the ATLAS detector using the 2015-2017 LHC proton-proton collision data*. 31 Jul. 2019. arXiv:1908.00005 [hep-ex].

[2] ATLAS Collaboration, *Measurements of the photon identification efficiency with the ATLAS detector using 4.9 fb1 of pp collision data collected in 2011*. ATLAS-CONF-2012-123.

[3] ATLAS Collaboration, *Search for new resonances decaying to pairs of merged diphotons in proton-proton collisions at s = 13 TeV*. 1 May. 2024. arXiv:2405.00834 [hep-ex].

[4] ATLAS Collaboration, *Search for short- and long-lived axion-like particles in H→aa→4 decays with the ATLAS experiment at the LHC*. 6 Dec. 2023. arXiv:2312.03306 [hep-ex].

[5] CERN, *Calorimeter | ATLAS Experiment at CERN*. 3 Nov. 2017.

[6] CERN, *Muon Spectrometer | ATLAS Experiment at CERN*. 2026.

[7] CERN, *The Inner Detector | ATLAS Experiment at CERN*. 2026.

[8] CERN, *The Standard Model*. 2026.

[9] CMS Collaboration, *Search for pairs of highly collimated photon-jets in pp collisions at s = 13 TeV with the ATLAS detector*. 30 Aug. 2019. arXiv:1808.10515 [hep-ex].

[10] Gabriel Matos and Lauren Larson and Abhilasha Dave and Maria Bressan and Azal Amer and Cindy Liu and Nikiforos Nikiforou and Jonathan Long and Timothy Andeen and John Parsons and Julia Gonski, *Transformer-based machine learning using low-level calorimeter signals for collimated photon identification at collider experiments*. 2026. arXiv:2607.08175 [hep-ph].

[11] Gregor Geßner on behalf of the ATLAS collaboration, *Photon identification with the ATLAS detector*. ATL-PHYS-PROC-2017-105.

[12] Martin Bauer, Matthias Neubert, Andrea Thamm, *Collider Probes of Axion-Like Particles*. 1 Aug. 2017. arXiv:1708.00443 [hep-ph].

[13] Nikiforos Nikiforou on behalf of the ATLAS collaboration, *Performance of the ATLAS Liquid Argon Calorimeter after three years of LHC operation and plans for a future upgrade*. 28 Jun. 2013. arXiv:1306.6756 [hep-ex].